



# A modeling approach integrating microbial activity, mass transfer, and geochemical processes to interpret biological assays: An example for PCE degradation in a multi-phase batch setup

Alexandra Marie Murray <sup>a</sup>, Julien Maillard <sup>b</sup>, Biao Jin <sup>c</sup>, Mette M. Broholm <sup>a</sup>,  
Christof Holliger <sup>b</sup>, Massimo Rolle <sup>a,\*</sup>

<sup>a</sup> Department of Environmental Engineering, Technical University of Denmark, Kgs. Lyngby, DK-2800, Denmark

<sup>b</sup> Laboratory for Environmental Biotechnology, ENAC-IIE, Ecole Polytechnique Fédérale de Lausanne, 1015 Lausanne, Switzerland

<sup>c</sup> State Key Laboratory of Organic Geochemistry, Guangzhou Institute of Geochemistry, Chinese Academy of Science, China

## ARTICLE INFO

### Article history:

Received 7 March 2019

Received in revised form

22 May 2019

Accepted 25 May 2019

Available online 27 May 2019

### Keywords:

Organohalide respiration

Microbial community

Sulfate and iron reduction

Multi-phase mass transfer

Biogeochemical modeling

IPhreeqc

## ABSTRACT

The rate at which organic contaminants can be degraded in aquatic environments is not only dependent upon specific degrading bacteria, but also upon the composition of the microbial community, mass transfer of the contaminant, and abiotic processes that occur in the environment. In this study, we present three-phase batch experiments of tetrachloroethene (PCE) degradation by a consortium of organohalide-respiring bacteria, cultivated alone or in communities with iron- and/or sulfate-reducers. We developed a modeling approach to quantitatively evaluate the experimental results, comprised of chemical and biomolecular time series data. The model utilizes the IPhreeqc module to couple multi-phase mass transfer between gaseous, organic and aqueous phases with microbial and aquatic geochemical processes described using the geochemical code PHREEQC. The proposed approach is able to capture the contaminant degradation, the microbial population dynamics, the effects of multi-phase kinetic mass transfer and sample removal, and the geochemical reactions occurring in the aqueous phase. The model demonstrates the importance of aqueous speciation and abiotic reactions on the bioavailability of the substrates. The model-based interpretation allowed us to quantify the reaction kinetics of the different bacterial guilds. The model further revealed that the inclusion of sulfate-reducing bacteria lowers the rate of PCE degradation and that this effect is moderated in the presence of iron-reducing bacteria.

© 2019 Elsevier Ltd. All rights reserved.

## 1. Introduction

Biodegradation of organic contaminants in aquatic systems depends not only on the activity and metabolic capabilities of specific degraders but also on microbial community interactions and on the coupling with mass transfer processes and aquatic chemistry. Microbial community function determines the fate of organic chemicals both in natural systems such as groundwater aquifers, riverbed sediments and hyporheic zones (Hamonts et al., 2012; Meckenstock et al., 2015; Weatherill et al., 2018), and in engineered applications, including *in-situ* bioremediation

\* Corresponding author. Department of Environmental Engineering, Technical University of Denmark, Bldg 115, 2800, Lyngby, Denmark.

E-mail address: [masro@env.dtu.dk](mailto:masro@env.dtu.dk) (M. Rolle).

interventions and wastewater treatment plants (e.g., Wells et al., 2011). Physical processes such as mass transfer between different phases, diffusion and hydrodynamic dispersion are also of key importance since they can be the rate-limiting step and thus the bottleneck for the degradation of organic compounds (e.g., Bauer et al., 2009a; Rolle et al., 2010; Rolle and Kitanidis, 2014; Thullner et al., 2012). Further control on contaminant biodegradation occurs through the feedback between microbial activity and abiotic reactions, including aqueous chemical speciation and precipitation/dissolution of reactive minerals (e.g., Appelo and Postma, 2005; Postma and Jakobsen, 1996; Prommer et al., 2009).

Chlorinated ethenes are organic contaminants of primary concern that are widespread in groundwater aquifers and threaten the health of riverbed sediments and surface water bodies (Imfeld et al., 2008; Schneidewind et al., 2014; Weatherill et al., 2018; Xu et al., 2019). The most important degradation pathway of

chlorinated ethenes is reductive dehalogenation by organohalide-respiring bacteria (OHRB), which can sequentially degrade the mother compounds such as tetrachloroethene (PCE) and trichloroethene (TCE), to daughter products *cis*-dichloroethene, vinyl chloride, and ultimately to the non-toxic ethene. This respiration process has been studied for more than two decades (Holliger et al., 1993), yet furthering understanding of how the interaction between microbial guilds, physical transport processes, and chemical reactions influences degradation kinetics can elucidate the functioning of degrader communities and will be instrumental to optimize bioremediation efforts.

Studying these systems *in situ* is difficult because microbial communities with relatively low biodiversity, such as those in groundwater sediments, can contain multiple thousands of taxa (Kotik et al., 2013). Hence, experimental studies with controlled conditions can increase our understanding of the interactions between different bacterial guilds (Marcus et al., 2013; Yu and Semprini, 2002). Cultivation of anaerobic microorganisms, both as pure cultures and as communities, is commonly done in small, septum-sealed, anoxic batches (Abe et al., 2009; Amos et al., 2007; Yu and Semprini, 2004). These systems allow for the bacterial community members to intermingle in the aqueous phase, which is key for microbial interactions, such as commensalistic OHRB-containing communities, in which the OHRB are dependent upon fermenting bacteria for production of electron donor. Another benefit of these systems is that a separate phase, such as a non-aqueous phase liquid or a gaseous atmosphere containing a toxic compound or a substrate, can be added to the setup. For organic contaminants such as chlorinated ethenes, an immiscible organic layer can be added to the system; the high partition coefficients for PCE and TCE means that these compounds preferentially remain in the organic phase, yet as organisms in the aqueous phase consume these chemicals, a chemical gradient is maintained and the organic layer acts as a source and slowly releases more substrate to the aqueous phase (Buttet et al., 2018; Holliger et al., 1993). Such slow, mass transfer limited release allows addressing the issue of bacterial inhibition by the toxicity of high substrate concentrations and increasing the experimental duration (Daugulis, 2001; Déziel et al., 1999).

These experimental systems are useful, but determining microbial kinetic parameters, such as affinity constants and maximum substrate utilization rates without accounting for the physical characteristics of the experimental system would lead to erroneous interpretation (Buttet et al., 2018). When substrate is metered out to the bacteria slowly and continuously, mass transfer across the phase boundaries (e.g., aqueous-organic and organic-gaseous) impacts the apparent substrate utilization rate, just as mass transfer limits bioavailability in natural systems (Aeppli et al., 2009; Bauer et al., 2009a; Kampara et al., 2008; Thullner et al., 2008). Sequential sampling also impacts the mass balance in the system. If an experimental system is small or if the amount of sample removed is relatively large, the removal of mass by this mechanism must also be considered since it affects the distribution of the different fluid phases in the setup (Buchner et al., 2016; Buttet et al., 2018).

Increasing the complexity of the bacterial community can also increase the complexity of the chemical reactions that occur in the aqueous phase (Gadd, 2010). To understand biodegradation kinetics one must determine the true concentration of the available substrate, thus the aqueous speciation of the substrates in the media needs to be accounted for. Furthermore, abiotic reactions between dissolved species and mineral precipitation/dissolution can impact microbial degradation processes. This is particularly important for microbial communities containing iron-reducing bacteria (FeRB) and sulfate-reducing bacteria (SRB), which entails

that iron-sulfur geochemical reactions occur. Although the focus is often the microbial degradation of the organic contaminants, there is continuous feedback between the aquatic geochemistry and microbial community that is essential to understanding community dynamics and, ultimately, the degradation process.

Although the experimental techniques described above are well-represented in the literature, the current state of numerical modeling for such systems does not cohesively incorporate these currently disparate elements. Modeling of multi-phase batch systems has previously been used to describe chlorinated ethene degradation and isotope fractionation, but these models do not include complex aquatic geochemistry (Aeppli et al., 2009; Buttet et al., 2018; Jin et al., 2013). Likewise, kinetic models to investigate batch or microcosm experiments of contaminant degradation and microbial communities account for neither mass transfer limitations nor the influence of sample removal on the determination of microbial kinetic parameters (Chambon et al., 2013; Jin and Rolle, 2016; Kouznetsova et al., 2010; Malaguerra et al., 2011; Wade et al., 2016).

In this study we present multi-phase microbial ecology experiments and a novel modeling tool used to interpret them that includes the description of mass transfer and geochemical processes. We performed laboratory batch experiments to investigate the impact of iron (Fe(III)) and sulfate reduction by FeRB and SRB on PCE reduction by an OHRB consortium containing *Candidatus Sulfurospirillum diekerktiae* strain SL2-1. The experiments consisted of four batches of increasing ecological complexity: the first batch consisted of the OHRB consortium cultivated alone, the second and third batches consisted of the OHRB consortium cultivated with either the FeRB or SRB, and the fourth batch consisted of all three guilds together. The proposed modeling approach is a coupling between a MATLAB<sup>®</sup>-based mass transfer code (Buttet et al., 2018) and the widely used geochemical code PHREEQC (Parkhurst and Appelo, 2013). We demonstrate the utility of this modeling tool to quantitatively interpret the experimental observations yielded by each batch, including both chemical and molecular data. The model allowed us to: (i) elucidate the impact of SRB and FeRB on PCE degradation, (ii) quantify the respiration kinetics of the different bacterial guilds, and (iii) disentangle the contribution of the different physical, biological, and chemical processes that occur in the multi-phase batch systems to the experimental observations, which consisted of measured time series of chemical and biomolecular data.

## 2. Materials and methods

### 2.1. Experiment

#### 2.1.1. Cultures

The OHRB consortium, SL2-PCEc, that was used in this study originated from a chlorinated ethene-contaminated aquifer and was enriched and maintained over several years (Buttet et al., 2013). The consortium contains *Candidatus Sulfurospirillum diekerktiae*, which is capable of respiring PCE to TCE. The FeRB used in the experiments was *Shewanella oneidensis* strain MR-1 (Heidelberg et al., 2002); the SRB used was *Desulfovibrio vulgaris* Hildenborough (Heidelberg et al., 2004). *S. oneidensis* and *D. vulgaris* were selected as model FeRB and SRB, respectively, because both can use hydrogen and neither can use acetate as an electron donor (Fredrickson et al., 2008; Tang et al., 2007; Tao et al., 2014).

#### 2.1.2. Experimental setup

The base medium used was phosphate-bicarbonate buffered with a low chloride concentration (Holliger et al., 1993), the

composition is listed in detail in Table S1. Medium components (chemicals sourced from Sigma-Aldrich Chemie GmbH, Buchs, Switzerland) and concentrated stocks were prepared with milliQ water and either autoclaved for 20 min at 121 °C or filtered through 0.22 µm sterile filters. All medium components were added to 125-mL autoclaved bottles sealed with butyl rubber stoppers using sterile syringes. Aliquots of 45 mL of base medium were prepared, and acetate, Fe(III)-citrate, and sulfate stock solutions were each added such that in the finished medium, 2 mM of carbon source, 5 mM of Fe(III) source, and 5 mM of sulfate source were present. The headspace was replaced with a 4:1 mixture of hydrogen to carbon dioxide through 0.22 µm sterile filters. The initial starting pressure of each bottle was approximately 1.5 atm; hydrogen was added to each batch in excess, and microbial activity is limited by the availability of the electron acceptor in this study.

After the replacement of the headspace and before inoculation, 5 mL of 100 mM PCE dissolved in hexadecane was added to the system. Because hexadecane has a lower density than and is immiscible with water, the hexadecane formed an organic layer between the aqueous and gaseous compartments in the bottle. PCE has a hexadecane-water partition coefficient of approximately 5000, thus the pre-inoculation aqueous concentration was 20 µM (Holliger et al., 1993). The bottles were allowed to sit for 24 h before inoculation, such that there was ample time for equilibration of PCE between the phases before introduction of the bacteria.

SL2-PCEc, *S. oneidensis*, and *D. vulgaris* were cultivated statically as separate inocula in a dark 37 °C room. The same cell count of the relevant guilds was added to each batch. Inoculation of the experimental batches was timed such that all inocula were in the exponential growth phase. All batch experiments were grown in the same conditions as the inocula. All combinations were conducted with biological duplicates. Samples of 1.5 mL were removed for analytical and molecular analyses. The samples were taken at regular intervals, with no more than 12 h between sample points, until constant chloride concentration values were obtained in all bottles, which occurred after 3.5 days.

### 2.1.3. Molecular methods

Cell counts of each guild inoculum, in order to match cell counts of inocula, were quantified by quantitative polymerase chain reaction (qPCR) using the universal primers detailed in the Supplementary Information. Analysis of qPCR data was performed on a MIC apparatus (Bio Molecular Systems). A standard curve was run in duplicate, and all samples were run in triplicate. PCR and terminal restriction length polymorphism (T-RFLP) sample analysis for each experimental batch were completed as described in the Supplementary Information. Although the T-RFLP analysis does not give absolute cell count values, it allows tracking of the temporal evolution of the entire community and verification that no unexpected population from the OHRB consortium appears during the experimental duration. Fragment counts were converted into cell counts by adjusting for the number of 16S rRNA gene copies per genome for each species (1 gene copy cell<sup>-1</sup> for *S. dieckertiae*, 5 gene copies cell<sup>-1</sup> for *D. vulgaris*, and 9 gene copies cell<sup>-1</sup> for *S. oneidensis*) (Buttet et al., 2018; Heidelberg et al., 2004, 2002).

### 2.1.4. Analytical methods

Fe(II) concentrations were measured using a colorimetric ferrozine assay (Viollier et al., 2000). Samples for ferrozine assay analysis were diluted ten times in 0.5 M HCl directly upon removal to prevent oxidation of Fe(II) to Fe(III) and to dissolve any Fe(II) precipitates (Zhou et al., 2017). Samples were not filtered, and thus the total Fe(II) concentration was measured. Chloride concentrations were determined via silver ion titration with a Chloro-counter (Flohr Instrument, Nieuwegein, Netherlands). Because

SL2-PCEc is only capable of transforming PCE to TCE, produced chloride is attributable to this single dechlorination step and PCE degradation can be measured without chlorinated ethene quantification (Buttet et al., 2018). Sulfate was measured by ion chromatography – suppressed conductivity detection (ICS-5000, Thermo Fisher). Samples were pretreated by passing them through a cleanup-cartridge (1 cc, Dionex OnGuard II Na, ThermoScientific) to remove divalent metal ions and protect the column and suppressor. Samples for sulfate analysis were diluted five times in a 5% zinc acetate solution directly upon removal to trap sulfide as zinc sulfide. Samples for sulfate analysis were frozen at –20 °C until analysis.

## 2.2. Modeling approach

The conceptual arrangement of the bacterial, multi-phase mass transfer, and aquatic geochemical processes that occur in the multi-phase experimental setup are schematically represented in Fig. 1. Mass transfer in the model is driven by both bacterial respiration (bolded and colored arrows, Fig. 1) and sample removal (block arrow, Fig. 1). In this section, we first describe each process individually and then present their combination in a modeling framework.

### 2.2.1. Bacterial kinetics

The bacterial processes (bolded and colored arrows, Fig. 1), are the primary driving force for mass transfer and transformations that occur during the experiment. Double Monod kinetics were used to simulate the consumption of both the electron donor and electron acceptors (Rittmann and McCarty, 2001):

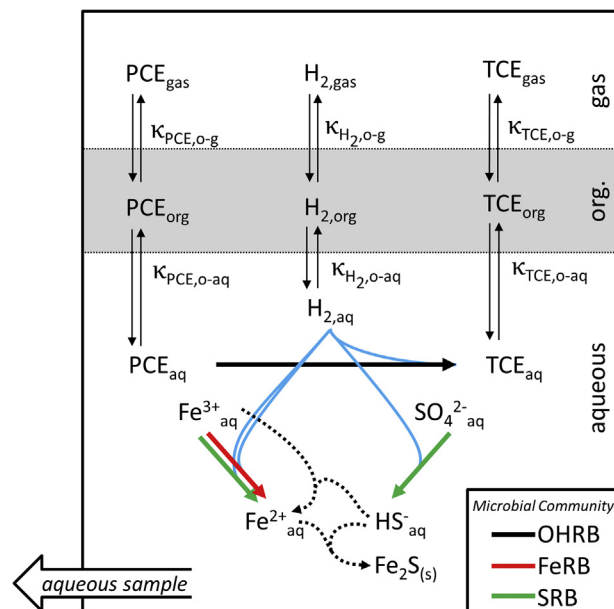


**Fig. 1.** Conceptual model of the physical, chemical, and bacterial processes that occur in the experimental setup, where  $k_{i,o-aq}$  is the mass transfer coefficient between the organic and aqueous phases, and  $k_{i,o-g}$  between the organic and gas phases, for compound *i*. The thick black arrow represents respiration by the OHRB *Candidatus* *Sulfurospirillum dieckertiae*, the thick red arrow respiration by the FeRB *Shewanella oneidensis*, and the thick green arrows respiration by the SRB *Desulfovibrio vulgaris*. Blue arrows represent pathways in which hydrogen is consumed. Slim black arrows represent mass transfer across phase boundaries. Dotted black lines represent aquatic geochemical reactions. The block arrow indicates that the aqueous phase is removed during sampling. (For interpretation of the references to color in this figure legend, the reader is referred to the Web version of this article.)

$$\frac{dC_{aq,EA}}{dt} = -k_{max}X \left( \frac{C_{aq,ED}}{C_{aq,ED} + K_{S,ED}} \right) \left( \frac{C_{aq,EA}}{C_{aq,EA} + K_{S,EA}} \right) \quad (1)$$

where  $dC_{aq,EA}/dt$  [mol L<sup>-1</sup> h<sup>-1</sup>] is the change in electron acceptor in the aqueous phase due to bacterial processes,  $C_{aq,ED}$  and  $C_{aq,EA}$  [μM] are the aqueous concentration of electron donor and acceptor,  $k_{max}$  [mol cell<sup>-1</sup> s<sup>-1</sup>] is the maximum specific reduction rate,  $X$  [cells L<sup>-1</sup>] is the biomass concentration,  $t$  [s] is time, and  $K_{S,ED}$  and  $K_{S,EA}$  [M] are the half-saturation constants for the electron donor and acceptor. The electron acceptors present in the media are PCE, Fe(III), and sulfate; hydrogen was the electron donor for all guilds. The change in substrate is related to biomass by:

$$\frac{dX}{dt} = Y_{EA} \frac{dC_{aq,EA}}{dt} - k_d X \quad (2)$$

where  $Y_{EA}$  [cells mol<sup>-1</sup>] is the biomass yield on the electron acceptor and  $k_d$  [s<sup>-1</sup>] is the linear decay coefficient. Equations (1) and (2) were applied for OHRB respiration of PCE to TCE, FeRB respiration of Fe(III) to Fe(II), and SRB respiration of sulfate to sulfide. *D. vulgaris*, the SRB used in the experiment, is also capable of respiring Fe(III). Elias et al. (2004) document this respiration to follow first-order kinetics, dependent only on the concentration of Fe(III), and both Elias et al. (2004) and Park et al. (2008) demonstrate that growth does not occur when reducing this metal ion. Fe(III) reduction by SRB was thus modeled by:

$$\frac{dC_{aq,Fe(III)}}{dt} = -k_{FeBio} C_{Fe(III),Bio} \quad (3)$$

where  $k_{FeBio}$  [s<sup>-1</sup>] is the first-order rate constant. The SRB *D. vulgaris* is modeled as capable of respiring both aqueous Fe(III) and sulfate, depicted by the green arrows in Fig. 1. The bioavailable Fe(III) is thus used as an electron acceptor by two guilds included in the experiments.

The hydrogen oxidation, cell synthesis, and PCE, Fe(III), and sulfate reduction half reactions (Table 1) were balanced using the method by Rittmann and McCarty (2001). The total stoichiometric reaction for each guild was obtained by a linear combination of the half reactions in Table 1:

$$R_{Total} = f_s(R_{Bio} + R_{ED}) + f_e(R_{EA} + R_{ED}) \quad (4)$$

where  $R_{Bio}$ ,  $R_{ED}$ , and  $R_{EA}$  are the half reactions for biomass synthesis, the electron donor, and the electron acceptor, respectively, and  $R_{Total}$  is the combined reaction.  $f_s$  and  $f_e$  are the fractions of electrons utilized for cell synthesis and energy production, respectively, which are calculated based on the yield factor,  $Y_{EA}$ , expressed as [mol<sub>biomass</sub> mol<sup>-1</sup>]. Moles of biomass are assumed to be represented by the formula C<sub>5</sub>H<sub>7</sub>O<sub>2</sub>N (Holliger et al., 1993) and each cell to have a mass of 1.72 × 10<sup>-13</sup> g cell<sup>-1</sup> (Balkwill et al., 1988). Growth does not occur during Fe(III) respiration by SRB, thus  $f_s$  for this

process is zero and all electrons are used for energy ( $f_e = 1$ ). For all other reactions, cell synthesis was modeled to occur via the same stoichiometry for all bacterial guilds. It has been found that approximately 70% of cell carbon for anaerobic bacteria is sourced from acetate and approximately 30% from CO<sub>2</sub> ( $R_{Bio}$ , Table 1) (Badziong and Thauer, 1978; Holliger et al., 1993). Fe(III) reduction by FeRB and SRB followed the same stoichiometry.

### 2.2.2. Multi-phase kinetic mass transfer

The movement of the electron donor and acceptor between the phases are represented by the slim, black arrows in the conceptual model (Fig. 1). The differential equations (5)–(7) describe the change in concentration of each relevant compound in each compartment by kinetic mass transfer (Aeppli et al., 2009; Jin et al., 2013):

$$\frac{dC_{aq,i}}{dt} = \frac{\left(\frac{dn_i}{dt}\right)_{gas-aq}}{V_{aq}} + \frac{\left(\frac{dn_i}{dt}\right)_{org-aq}}{V_{aq}} \quad (5)$$

$$\frac{dC_{org,i}}{dt} = \frac{-\left(\frac{dn_i}{dt}\right)_{org-aq}}{V_{org}} + \frac{-\left(\frac{dn_i}{dt}\right)_{org-gas}}{V_{org}} \quad (6)$$

$$\frac{dC_{gas,i}}{dt} = \frac{-\left(\frac{dn_i}{dt}\right)_{gas-aq}}{V_{gas}} + \frac{\left(\frac{dn_i}{dt}\right)_{org-gas}}{V_{gas}} \quad (7)$$

where  $dC_{p,i}/dt$  [mol L<sup>-1</sup> s<sup>-1</sup>] is the change in concentration for the compound,  $i$ , in phase,  $p$ ,  $V_p$  [L] is the volume of phase  $p$ , and  $dn_i/dt$  [mol s<sup>-1</sup>] is the total change in moles between phases for the compound. PCE, TCE, and hydrogen were modeled to move between the phases, and movement from the organic phase is defined as positive. Hydrogen concentrations were calculated based on the known initial pressure in and fractional composition of the headspace and the ideal gas law. The movement of mass across the two relevant phase interfaces,  $(dn_i/dt)_{org-aq}$  and  $(dn_i/dt)_{org-gas}$ , is described by Equations (8) and (9) (Aeppli et al., 2009):

$$\left(\frac{dn_i}{dt}\right)_{org-aq} = V_{aq} \left( C_{aq,i}^{eq} - C_{aq,i} \right) \left( \frac{\kappa_{org-aq,i} \cdot A}{V_{org}} \right) \quad (8)$$

$$\left(\frac{dn_i}{dt}\right)_{org-gas} = V_{gas} \left( C_{gas,i}^{eq} - C_{gas,i} \right) \left( \frac{\kappa_{org-gas,i} \cdot A}{V_{org}} \right) \quad (9)$$

where  $C_{p,i}$  [M] and  $C_{p,i}^{eq}$  [M] are the concentration and equilibrium concentration of compound  $i$  in phase  $p$ ,  $\kappa_{org-aq,i}$  [dm s<sup>-1</sup>] and  $\kappa_{org-gas,i}$  [dm s<sup>-1</sup>] are the mass transfer coefficients for compound  $i$ , and  $A$  [dm<sup>2</sup>] is the cross-sectional area of the phase interface. Mass transfer coefficients can be found in Table S2.

### 2.2.3. Sample Removal

Sample removal and re-equilibration of PCE, TCE, and hydrogen was also included in the model. Sampling removes substrate from the system, and it has previously been found to increase the chloride concentration in the aqueous phase above what would have been possible without removal of the aqueous phase (Buttet et al., 2018). Additionally, removal of phase volume from the system affects the pressure in the batch bottle. Equilibration of the volatile compounds was modeled as occurring instantaneously after sample removal. The total moles of the compound remaining in the system at time  $t$ , after sample removal, was calculated by subtracting the moles in the aqueous sample removed at time  $t$  from the moles present before removal at time  $t-1$ :

**Table 1**  
Stoichiometry for respiration and cell synthesis half reactions.

Reaction	Stoichiometry
$R_{ED}$	$\frac{1}{2}H_2 \rightarrow H^+ + e^-$
$R_{Bio}$	$\frac{1}{2}CH_3COO^- + \frac{1}{4}CO_2 + \frac{1}{4}NH_4^+ + \frac{5}{4}H^+ + e^- \rightarrow \frac{1}{4}C_5H_7O_2N + H_2O$
$R_{EA}$ : PCE	$\frac{1}{2}C_2Cl_4 + H^+ + e^- \rightarrow \frac{1}{2}C_2HCl_3 + \frac{1}{2}H^+ + \frac{1}{2}Cl^-$
$R_{EA}$ : Fe <sup>3+</sup>	$Fe^{3+} + e^- \rightarrow Fe^{2+}$
$R_{EA}$ : SO <sub>4</sub> <sup>2-</sup>	$\frac{1}{8}SO_4^{2-} + \frac{19}{16}H^+ + e^- \rightarrow \frac{1}{16}H_2S_{(g)} + \frac{1}{16}HS^- + \frac{1}{2}H_2O$

$$n_{i,t} = (C_{gas,i}V_{gas} + C_{org,i}V_{org} + C_{aq,i}V_{aq})_{t-1} - (C_{aq,i}V_{s,aq})_t \quad (10)$$

where  $n_{i,t}$  [mol] is the remaining mass of compound  $i$  and  $V_{s,aq}$  [L] is the volume of the removed sample. The concentrations of the compound in each phase after sample removal was then calculated (Buchner et al., 2016) using the partition coefficients  $K_{gas-org}$  and  $K_{org-aq}$  [-] (Table S2).

#### 2.2.4. Geochemistry

The iron and sulfide chemistry in the aqueous phase both affects and is affected by the microbial reduction processes. The aqueous chemistry directly affects these bacterial processes via the speciation, and consequently the bioavailability, of the Fe(III) electron acceptor (Haas and Dichristina, 2002; Liu et al., 2001). Both the SRB and FeRB were modeled as only able to respire aqueous Fe(III) ions and the Fe(III) hydroxyl complexes  $Fe(OH)_3$ ,  $Fe(OH)_2^+$ , and  $Fe(OH)_4^-$ . Fe(III) was added to the media as Fe(III)-citrate, which was modeled in PHREEQC to speciate according to the reactions included in Table 2.

Geochemical reactions in the system, depicted in Fig. 1 as dotted lines, are also driven by the bacterial processes. Fe(III) reacts abiotically with sulfide, a product of sulfate reduction, by the stoichiometric reaction and rate kinetics described in Equations (11) and (12), respectively:



$$\frac{dC_{Fe(II)}}{dt} = k_{FeAbio} C_{Fe(III)} C_{S(-II)}^{0.5} \quad (12)$$

where  $k_{FeAbio}$  [ $L^{0.5} mol^{-0.5} s^{-1}$ ] is the kinetic rate constant for Fe(II) production as a result of abiotic Fe(III) reduction (Poulton et al., 2004; Rickard and Luther, 2007). The rate of abiotic Fe(III) reduction has been determined to be first order with respect to Fe(III) and 0.5 order with respect to sulfide (Poulton et al., 2004). The produced Fe(II) then also reacts with sulfide to form amorphous  $FeS_{(s)}$  that later crystallizes to mackinawite (Remoundaki et al., 2008; Zhou et al., 2017, 2014). When sulfide concentrations are high ( $10^{-5}$  M or greater) and the pH is neutral, Rickard (1995) found that this precipitation reaction proceeds by a reaction between Fe(II) and sulfide, where  $FeS_{(s)}$  is formed via the intermediate  $Fe(HS)_{2(s)}$  mineral with an empirically determined pseudo first-order sulfide disappearance rate of  $15 s^{-1}$  (Rickard, 1995). Because the formation of the FeS precipitate is quick and the duration of the experiment was not long enough for crystallized mackinawite to form, amorphous  $FeS_{(s)}$  was allowed to precipitate in the model at equilibrium via the reaction (Jakobsen, 2007):



**Table 2**  
Fe(III)-citrate speciation reactions included in the PHREEQC database.

Reaction	Log(k)
$Fe^{3+} + Citrate^{3-} + H_2O \rightarrow FeCitrateOH^- + H^+$	9.98 <sup>a</sup>
$Fe^{3+} + Citrate^{3-} \rightarrow FeCitrate$	12.55 <sup>b</sup>
$Fe^{3+} + 2Citrate^{3-} + H_2O \rightarrow FeCitrate_2OH^{4-} + H^+$	13.42 <sup>a</sup>
$Fe^{3+} + Citrate^{3-} + H^+ \rightarrow FeCitrateH^+$	19.8 <sup>b</sup>
$Fe^{3+} + 2Citrate^{3-} + 2H^+ \rightarrow FeCitrate_2H_2^-$	26.46 <sup>a</sup>

<sup>a</sup> Reaction and log(k) as described in Liu et al. (2001).

<sup>b</sup> Reaction and log(k) from the PHREEQC minteq.dat database.

where the log of the equilibrium constant, log(k), for  $FeS_{(s)}$  was used from the PHREEQC geochemical database.

#### 2.2.5. Coupling strategy

The bacterial, mass transfer, consecutive sample removal, and aqueous chemistry modeling components are linked together via the scheme presented in Fig. 2. Two software platforms are used, MATLAB® (R2017b) and PHREEQC-3 (Parkhurst and Appelo, 2013). The IPhreeqc module (Charlton and Parkhurst, 2011), allowing the use of PHREEQC with other codes and scripting languages (Muniruzzaman and Rolle, 2016; Van Breukelen et al., 2017; Wissmeier and Barry, 2011), was employed to interface the two software platforms. The mass transfer processes and re-equilibration after sample removal were performed in MATLAB®, analogous to the transport steps in reactive transport models using an operator splitting approach (e.g., Muniruzzaman and Rolle, 2016; Rolle et al., 2018). The state of the aqueous phase after these processes was then communicated to the PHREEQC geochemical code using the IPhreeqc module. All biogeochemical processes including aqueous speciation, homogeneous and heterogeneous reactions, contaminant degradation and bacterial population dynamics were performed by PHREEQC. The flexible coupling strategy allowed us to perform simulations mimicking the steps taken in the laboratory experiments, as illustrated in Fig. 2. First, the media was assembled and the volatile compounds equilibrated between all phases (Point A). The bacterial inocula were then added to each experimental batch (Point B), and an initial sample was removed and the volatile compounds re-equilibrated (Point C).

Equilibration after the initial sample is removed begins the outer of two nested loops. The outer loop is organized in discrete segments, the length of which is defined by the time between the experimental sampling events. Point D is prior to and Point C is directly after sample removal. To move from Point C to D, the model enters the inner of the two nested loops. To return to Point C from Point D, the volume of the aqueous phase is decreased by the size of the sample volume and the volatile compounds are re-equilibrated between the phases.

After a sample is removed, the inner of the two nested loops begins. This inner loop is based on an operator splitting scheme that alternates between the PHREEQC and MATLAB® platforms with a small coupling time step (i.e.,  $\Delta t = 5$  s). To move from Point E to F, the bacterial and geochemical processes proceed in PHREEQC. After each time step, the model arrives to Point F, and the

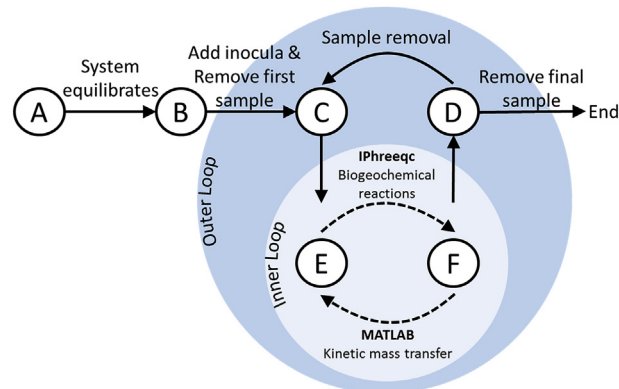


**Fig. 2.** Coupling strategy for MATLAB® and PHREEQC software platforms; the bacterial and aqueous chemical processes are computed using PHREEQC and the instantaneous and kinetic mass transfer processes are completed using MATLAB®. Solid black arrows denote steps that are modeled to occur instantaneously, and dashed arrows denote continuous processes that proceed for a defined time length.

concentrations of the volatile compounds in the aqueous phase are passed to MATLAB<sup>®</sup>, which solves the set of differential equations to describe kinetic mass transfer between the phases with the stiff solver *ode15s*. The concentrations of the volatile compounds are returned to PHREEQC at Point E and the loop repeats. When the next sample is to be removed, the concentrations of the volatile compounds at Point F are returned to MATLAB<sup>®</sup> at Point D, a sample is removed, and the next iteration of the outer loop begins at Point C. Removal of the last sample signals the end of the outer loop.

### 2.2.6. Parameter fitting

The model was applied to the performed experiments to interpret the chemical and molecular data in all the experimental batch setups that we have considered with the aim of quantifying the kinetics of the different microbial guilds. As many parameters were chosen from the literature as possible to limit the number of parameters to be fitted to the  $k_{max}$  for each guild's respiration process. Parameter fitting was conducted within the MATLAB<sup>®</sup> environment using the function *lsqnonlin* (e.g., Haberer et al., 2015). The OHRB initial cell count was fitted for each experimental batch to account for unknown activity of the inoculum, in which the upper bound was the measured initial count,  $1.02 \times 10^8$  cells L<sup>-1</sup>.  $k_{max}$  was fitted for all bacterial guilds in all experimental batches. In the batch that included OHRB and FeRB,  $K_{S,FeRB,Fe3}$  was also fitted, as values found in the literature were for the total dissolved Fe(III) concentration, not the easily bioavailable dissolved Fe(III) concentration (Liu et al., 2001). Parameters fit to describe 2-part community batch configurations, e.g.,  $K_{S,FeRB,Fe3}$  and  $k_{FeAbio}$ , were used as fixed inputs in subsequent, 3-part community batch simulations.

## 3. Results and discussion

The four experimental configurations are detailed in Table 3. From left to right, each column gives the details of the batches as they increase in complexity. Batch 1, the single-community consisting of the OHRB consortium, is used to demonstrate the utility of the model as it relates to mass transfer across the phase boundaries and replicating sequential sample removal. Batch 2, the community consisting of OHRB and FeRB, shows how multiple guilds can be simulated. Aqueous speciation is modeled in all batches, and Batch 2 demonstrates that the Fe(III) bioavailability directly impacts iron respiration. Batch 3 is still comprised of two guilds, OHRB and SRB, and includes the complex aquatic geochemical processes that result

from sulfate reduction products. Finally, Batch 4 is the most complex configuration, and consists of all three guilds and biogeochemical reactions considered. Data and simulations for each batch duplicate are included in the SI. In all simulations, the fitted initial cell count was found to vary in an interval spanning less than half an order of magnitude (i.e., with a minimum of  $5.93 \times 10^7$  cells L<sup>-1</sup>), indicating the added cultures were proportionally and initially active.

### 3.1. Single Community: Organohalide-Respiring Bacteria

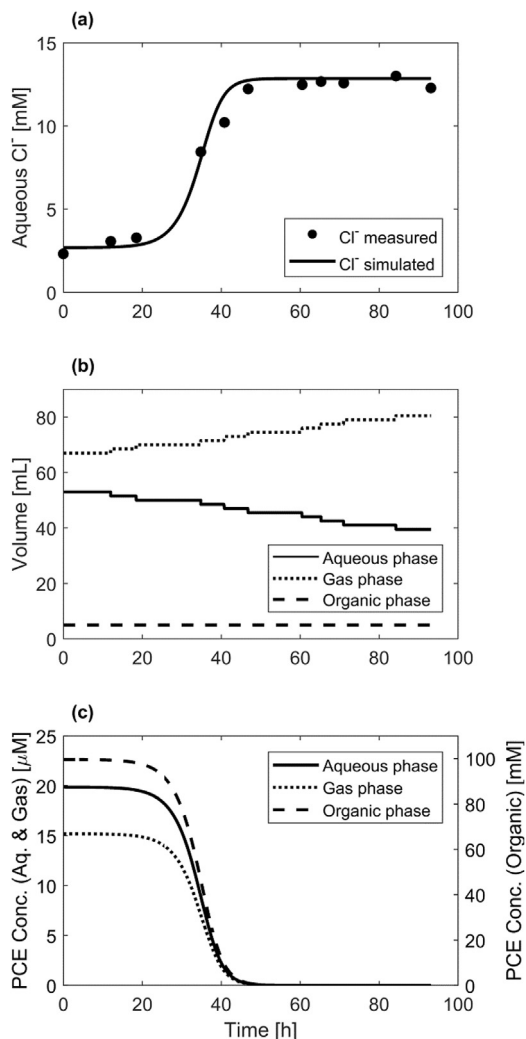
In Batch 1, the OHRB consortium was cultivated without any other functional guild, and thus the chloride data is most relevant, as it is the product of PCE respiration. Repeated chloride concentration values from approximately 48 h indicate that all PCE consumption stopped at this time. The model was able to simulate the sigmoid curve of the measured chloride (Fig. 3a) and thus capture PCE dechlorination to TCE and subsequent growth of OHRB. The  $k_{max,PCE}$  for the OHRB in Batch 1 and its biological duplicate were  $4.50 \times 10^{-18}$  and  $4.01 \times 10^{-18}$  mol<sub>PCE</sub> cell<sup>-1</sup> s<sup>-1</sup> (Table 4), which is one order of magnitude greater than the average value found during previous experiments with the same consortium (Buttet et al., 2018) and also in other studies with members of the same organohalide-respiring genus (Aeppli et al., 2009; Scholz-Muramatsu et al., 1995). This can be attributed to the difference of electron donor, as formate was used as the electron donor in Buttet et al. (2018), and supply of hydrogen has been shown to best promote dechlorination (Aulenta et al., 2007).

Fig. 3b depicts the calculated volume of each phase throughout the experiment. Even with a minimal sampling volume of 1.5 mL, it is still evident that consecutive sampling has a considerable impact on the phase volumes of the batch system. The initial volume of the aqueous phase decreased by 18% (and the volume of the gas phase increased by the same volume) over the duration of the experiment. The initial pressure in the bottle was approximately 1.5 atm, determined when the headspace was exchanged prior to addition of the organic phase during preparation of the experiment. At the end of the experiment, because of sample removal and consumption of PCE and hydrogen, the calculated pressure in the batch was 1.0 atm. Additionally, the model allows us to track the evolution of the volatile species in all phases (Fig. 3c, example for PCE). It was determined that the electron donor was present in excess in the aqueous phase; the lowest aqueous hydrogen concentration in the

**Table 3**

Overview of the experiments, including guilds added to the batch and the processes and data that are relevant to each batch.

Batch	Single Community		Two-part Community		Three-part Community
	1	2	3	4	
<b>Guilds</b>	OHRB	OHRB FeRB	OHRB  SRB	OHRB FeRB SRB	
<b>Relevant Processes</b>	<b>Biotic</b>      <b>Abiotic</b>	PCE reduction      Fe(III) speciation	PCE reduction Fe(III) reduction (FeRB)   Fe(III) speciation Fe(III) reduction FeS <sub>(s)</sub> precipitation	PCE reductions Sulfate reduction Fe(III) reduction (SRB)  Fe(III) speciation Fe(III) reduction FeS <sub>(s)</sub> precipitation	
<b>Relevant Data</b>	Chloride	Chloride Fe(II) T-RFLP	Chloride Fe(II) T-RFLP Sulfate	Chloride Fe(II) T-RFLP Sulfate	



**Fig. 3.** OHRB only (Batch 1) experimental and simulated chloride aqueous concentration (a), phase volume changes due to sampling (b), and simulated decrease of PCE in all phases (c). Data and simulation results for the biological duplicate are included in the Supplementary Information (Fig. S1).

batch was  $5.35 \times 10^{-4}$  M. The model shows that the PCE concentration in all three phases is zero after approximately 48 h. This coincides with the repeated chloride concentration values and simulation (Fig. 3a) that indicate PCE respiration has stopped, with complete PCE consumption in the system after 48 h.

### 3.2. Two-part community: organohalide- and Fe(III)-Respiring bacteria

In Batch 2, the two-part community composed of the OHRB consortium and FeRB (Table 3 Batch 2), chloride and Fe(II) are respiration products that can be used as evidence of the functional guilds' metabolic activity. The chloride sigmoid data and simulation for Batch 2 is similar to Batch 1, with the OHRB alone, and repeated chloride concentration values were also observed after approximately 48 h (Fig. 4a).

The Fe(II) concentration increases rapidly within the first 24 h of the experiment, and then increases slowly throughout the rest of the experimental duration (Fig. 4b). The concentration of Fe(II) obtained at approximately 48 h, when PCE reduction was complete, is less than the Fe(III) concentration added as Fe(III)-citrate because of Fe(III) speciation in the medium. Fe(II) reduction is still ongoing

at this time, since after the initial equilibration of the solution, less than 4% of the Fe(III) was in a form that could be used by the bacteria. This phenomena has previously been observed in experiments using a related bacterial strain (*Shewanella putrefaciens* strain CN32), in which a half-velocity constant,  $K_{S,FeRB,Fe3}$ , was determined to be  $2.9 \times 10^{-3}$  M, based on the total Fe(III) concentration and with lactate as the electron donor and carbon source (Liu et al., 2001). The  $K_{S,FeRB,Fe3}$  fit to our experiment were found to be  $7.93 \times 10^{-5}$  and  $7.26 \times 10^{-5}$  M in Batch 2 and its biological duplicate. These values are two orders of magnitude lower, which is consistent with the difference in magnitude between the bioavailable (this study) and total (Liu et al., 2001) concentrations of the electron acceptor.

Because this batch includes multiple community members, the T-RFLP data shows the change in the community over the duration of the experiment. Fig. 4c and d show that the FeRB dominate the community for the first 24 h of the experiment, and the OHRB dominate throughout the rest of the experimental duration. This correlates well with the rapid FeRB growth in the first 24 h of the experiment and the rapid OHRB growth between 24 and 40 h of the experiment. The model, including the dynamics of the OHRB and FeRB, could well capture the observed molecular data and the shift in dominance between the two microbial guilds during the time-frame of the experiment.

### 3.3. Two-part community: organohalide- and sulfate-respiring bacteria

Batch 3, the two-part community that contained OHRB and SRB (Table 3 Batch 3), inherently contained more processes than the previous batches; the selected SRB bacteria is metabolically versatile and the products from sulfate reduction react with Fe(III) and Fe(II). The model was again able to simulate the sigmoid chloride accumulation curve (Fig. 5a), and in this batch, repeated chloride concentration values were obtained after approximately 60 h. The sulfate concentration (Fig. 5b) decreases slowly for the first 60 h of the experiment before decreasing rapidly between approximately 60 and 65 h. This sulfate consumption by the SRB is reproduced well using the kinetic constants determined by previous experiments (Noguera et al., 1998) that used hydrogen as an electron donor. The relative abundance data (Fig. 5d and e) show that OHRB steadily become dominant throughout the duration of the experiment. The simulation of the relative abundance data captures the general trend, in particular the repeated data points at the end of the T-RFLP time series data, which indicates that the model is able to capture the relative growth of the two guilds based on their yields once their electron acceptors have been completely consumed.

The Fe(II) concentration measurements in Batch 3 (Fig. 5c) appears to show two periods of fast accumulation, the first within 0–20 h and the second within 60–70 h. This is in contrast to the Fe(II) accumulation curve that results from Fe(III) respiration from FeRB in Batch 2 (Fig. 4b), which only showed an initial concentration increase in the first 24 h. In Batch 3, both biotic and abiotic Fe(III) reduction to Fe(II) take place, and each process accounts for one of these observed increases. Fig. 5c demonstrates how neither abiotic nor biotic Fe(III) reduction alone is able to account for the measured Fe(II) concentration, and that the Fe(II) accumulation curve is a composite of two Fe(III) reduction processes. During the first 18 h of the experiment, the Fe(II) concentration has risen by 1.2 mM and the sulfate concentration has decreased by 0.1 mM. Since 2 mol of Fe(II) are produced per mole of sulfide consumed during abiotic Fe(III) reduction (Equation (11)), another process must be responsible for the observed increase in Fe(II). Likewise, if only first-order biotic Fe(III) reduction by SRB is included in the model, then the elevated Fe(II) measurements at the end of the

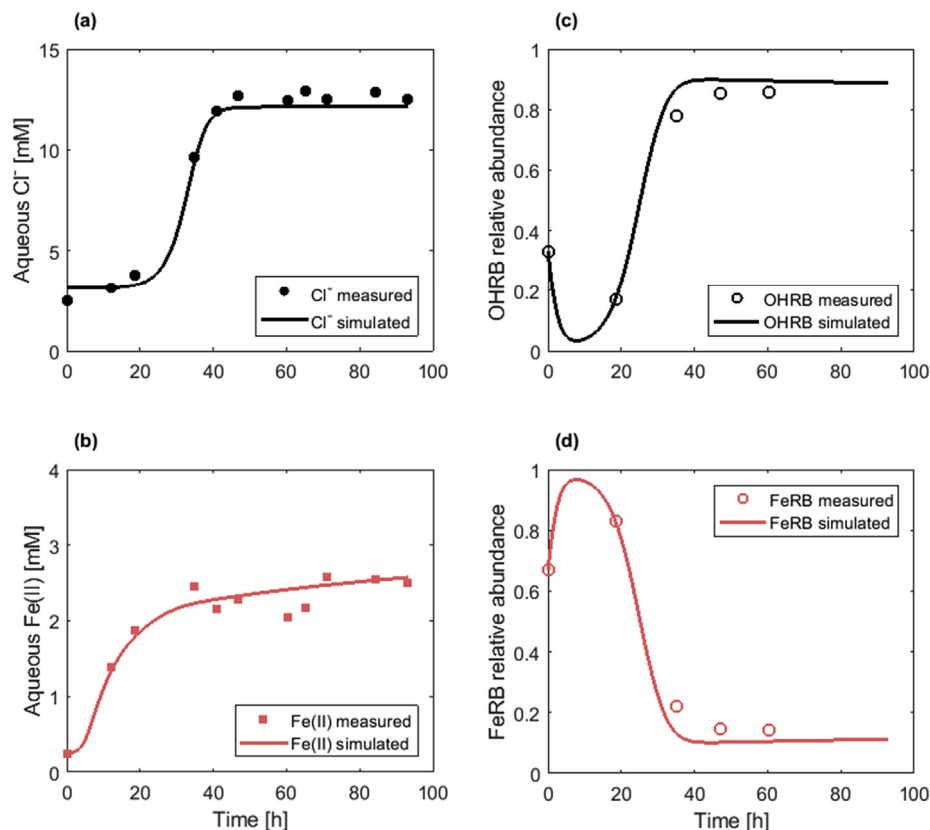


**Fig. 4.** OHRB and FeRB (Batch 2) experimental and simulated chloride and Fe(II) aqueous concentrations (a and b) and OHRB and FeRB relative abundance (c and d). Data and simulation results for the biological duplicate are included in the Supplementary Information (Fig. S2).

time series are unable to be captured.

The SRB used in this experiment is capable of both Fe(III) and sulfate reduction. Biotic degradation of Fe(III) by *Desulfovibrio* sp. has been documented to not result in cell synthesis and can be modeled as a first-order process dependent on the concentration of bioavailable Fe(III) (Elias et al., 2004). It has been posited that *Desulfovibrio* sp. reduce Fe(III) because it is a more favorable electron acceptor (Zhou et al., 2017) or as protection against cell oxidation by compounds with a higher redox potential than that of sulfate (Cypionka, 2000; Elias et al., 2004). Regardless of the objective, it is evident that Fe(III) reduction proceeds first, followed by an apparent acceleration of sulfate reduction after approximately 60 h.

The model also allows the simulation of the chemical reactions that occur as a result of sulfide production via SRB respiration (Fig. 5f). Though only the total Fe(II) concentration was quantified, the formation of black precipitate in those batches that contained SRB was observed after 24 h. The formation of precipitate was simulated using the standard thermodynamic PHREEQC database; the model corroborates what is visually observed and also shows that amorphous mackinawite, or FeS<sub>(s)</sub>, begins to form after approximately 20 h. The simulation of Batch 3 shows that although sulfate reduction does occur relatively slowly throughout the first 40 h of the experiment (Fig. 5b), FeS<sub>(s)</sub> is not the primary form of Fe(II) until after approximately 60 h of SRB growth. When sulfate is nearly depleted, all measured Fe(II) is bound as FeS<sub>(s)</sub>.

### 3.4. Three-part community: organohalide-, Fe(III)-, and sulfate-respiring bacteria

In Batch 4, all three guilds were cultivated together (Table 3 Batch 4), and all processes that were observed in each previous

batch occurred together. The inoculum for this batch was comprised of the three guilds such that the initial cell count of each guild was the same as in the other three batches. Even when all three guilds are present, electron donor is still supplied in excess, and the lowest aqueous hydrogen concentration was  $2.31 \times 10^{-4}$  M.

The sigmoidal chloride accumulation curve in Batch 4 (Fig. 6a) is similar to those in Batches 1 (Figs. 3a) and 2 (Fig. 4a), as repeated concentration values were observed after approximately 48 h. The Fe(II) measurements (Fig. 6c) are similar to those found in Batch 3 (Fig. 5c), in that there is a relatively fast increase to a concentration of about 2 mM within the first 20 h, and a second relatively fast increase in concentration at about 60 h. The sulfate curve, however, is slightly different in Batch 4 (Fig. 6b) than in Batch 3 (Fig. 5b). Although the sulfate disappears from the experiment at approximately 70 h in both batches, the decrease in measured sulfate appears to begin earlier and is more gradual in Batch 4 than in Batch 3. The model is able to accurately simulate both the chloride and sulfate curves as well as the Fe(II) composite curve.

The T-RFLP relative abundance data show that the OHRB gradually grow to dominate the microbial community throughout the time series while the SRB maintain a more or less steady proportion and the FeRB rapidly decline to become a small proportion of the community. Just as in Batches 2 and 3, the proportional community measurements (Fig. 6d, e, and f) at the end of the time series, after approximately 65 h, are captured for all three guilds, which is consistent with the yield factors of the different guilds. More difficulties were encountered in the simulation of the transient measurements of the community development. The model allows capturing the decrease of FeRB, but overestimates the transient relative abundance for OHRB and underestimates for SRB. This discrepancy may be because of the relative nature of the



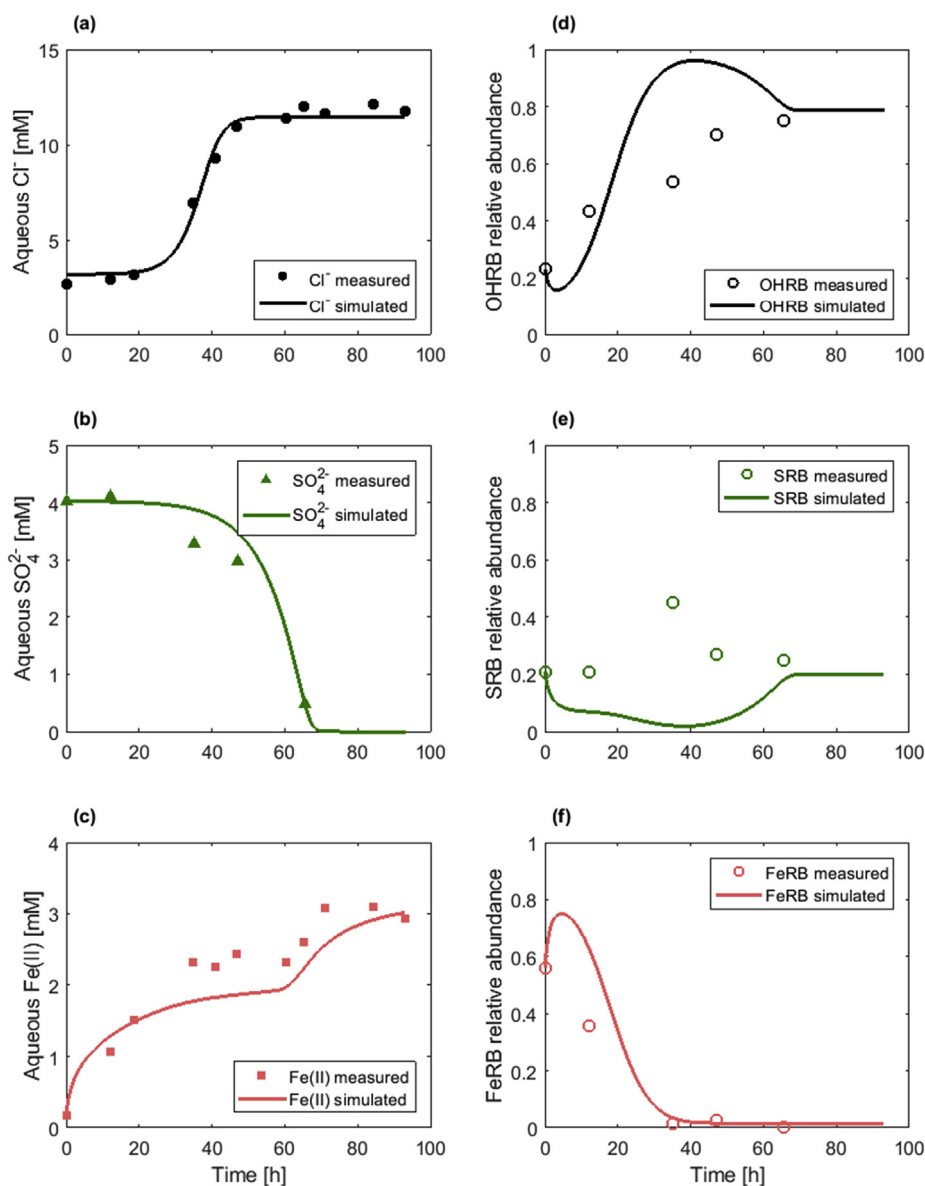


**Fig. 6.** OHRB, SRB, and FeRB (Batch 4) experimental and simulated chloride, sulfate, and total Fe(II) aqueous concentrations (a, b, and c) and OHRB, SRB, and FeRB relative abundance (d, e, and f). Data and simulation results for the biological duplicate are included in the Supplementary Information (Fig. S4).

When comparing Batches 1 and 2, in which the OHRB consortium was present alone and in combination with FeRB (Fig. 7a and b), it is evident that there is no appreciable difference between the degradation of PCE when the FeRB are and are not present, as the shape of the PCE consumption peak is similar in both shape and

height in both batches. The OHRB appear to behave no differently whether reduction by FeRB occurs or not. This may be due to the Fe(III) speciation and subsequent electron acceptor bioavailability limitation on FeRB respiration.

The OHRB behavior in Batch 3 is noticeably different from that of

**Table 4**

Estimated parameters for each batch; duplicates are given in the second row; data and simulations for duplicates are included in the SI.

Parameter		$k_{max,OHRB}$ $\text{mol}_{PCE} \text{ cell}^{-1} \text{ s}^{-1}$	$k_{max,FeRB}$ $\text{mol}_{Fe3} \text{ cell}^{-1} \text{ s}^{-1}$	$k_{max,SRB}$ $\text{mol}_{SO4} \text{ cell}^{-1} \text{ s}^{-1}$	$K_{S,FeRB,Fe}$ $\text{mol}_{Fe3} \text{ L}^{-1}$	$K_{S,SRB,SO4}$ $\text{mol}_{SO4} \text{ L}^{-1}$	$k_{FeAbio}$ $\text{L}^{0.5} \text{ mol}^{-0.5} \text{ s}^{-1}$
<b>Batch 1</b>	1	$4.50 \times 10^{-18}$	–	–	–	–	–
	2	$4.01 \times 10^{-18}$	–	–	–	–	–
<b>Batch 2</b>	1	$4.82 \times 10^{-18}$	$1.82 \times 10^{-17}$	–	$7.93 \times 10^{-5}$	–	–
	2	$4.80 \times 10^{-18}$	$1.97 \times 10^{-17}$	–	$7.26 \times 10^{-5}$	–	–
<b>Batch 3</b>	1	$2.93 \times 10^{-18}$	–	$8.40 \times 10^{-18}$	–	–	$2.97 \times 10^{-4}$
	2	$3.35 \times 10^{-18}$	–	$8.11 \times 10^{-18}$	–	–	$4.31 \times 10^{-4}$
<b>Batch 4</b>	1	$4.13 \times 10^{-18}$	$2.18 \times 10^{-17}$	$8.45 \times 10^{-17}$	–	$3.51 \times 10^{-4}$	–
	2	$3.98 \times 10^{-18}$	$1.68 \times 10^{-17}$	$1.60 \times 10^{-17}$	–	$2.91 \times 10^{-3}$	–

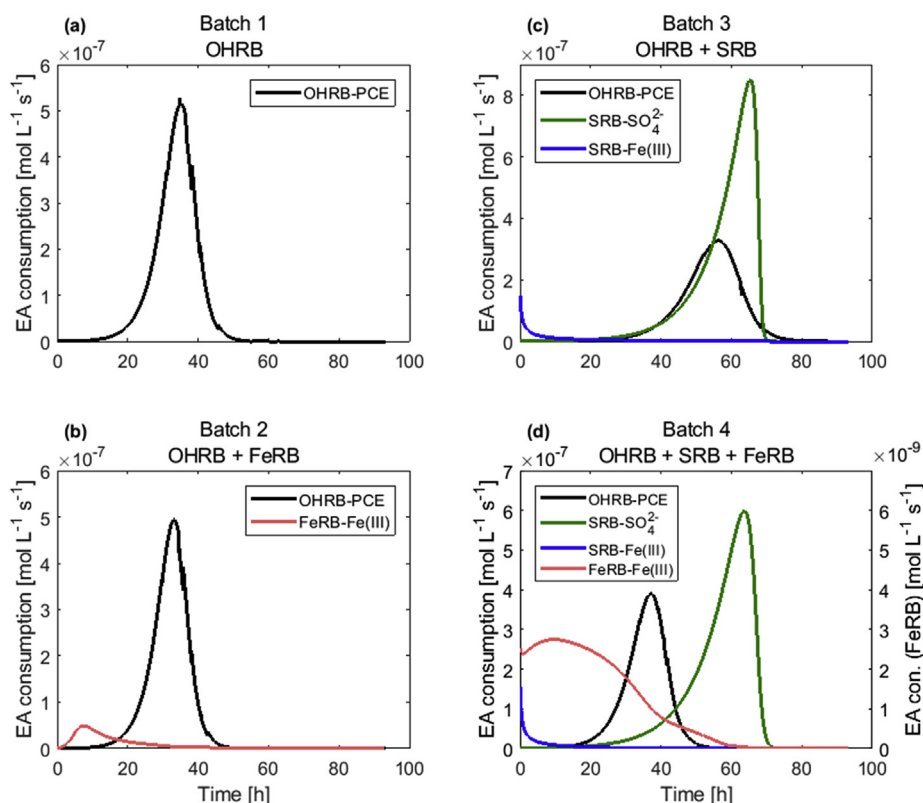


Fig. 7. Consumption rates for electron acceptors, Batch 1: OHRB (a), Batch 2: OHRB + FeRB (b), Batch 3: OHRB + SRB (c), and Batch 4: OHRB + FeRB + SRB (d).

Batches 1 and 2 (Fig. 7c). It is evident that PCE degradation proceeds much less rapidly, as the maximum specific rate of PCE consumption is 65% of that observed in Batch 1 and 61% of that observed in Batch 2 (Fig. 7a and b). The OHRB only begin to consume PCE concurrently with sulfate consumption as shown by the simulated rate curves of the 2 bacterial guilds. Such a correlation between PCE degradation and sulfate reduction has also been found in other studies (Aulenta et al., 2008; Berggren et al., 2013; Mao et al., 2015). Furthermore, in Batch 4 (Fig. 7d) it appears that Fe(III) reduction by FeRB can enhance PCE reduction by OHRB, although the maximum specific degradation rate is still subdued compared to that of Batches 1 and 2. This may highlight the necessity to consider the biodiversity of the entire microbial community during bioremediation application (Aulenta et al., 2007), rather than focus on organohalide-respiring bacteria.

#### 4. Conclusion

In this study we have proposed a modeling approach, based on MATLAB<sup>®</sup>-PHREEQC coupling, to interpret biological assays in which microbial dynamics, mass transfer processes, and geochemical reactions can affect the degradation of organic contaminants. We performed batch experiments of increasing ecological complexity on the impact of iron and sulfate reduction on PCE reductive dehalogenation, and we used the proposed model to interpret the experimental observations. The model allowed us to quantify the kinetics of the different bacterial guilds and to quantitatively evaluate the effects of the physical, chemical and biological processes that occurred in the multi-phase batch setups. Furthermore, the model could calculate the respiration rate throughout the experimental duration, and thus the change in rate could be depicted and compared across different community compositions. The rate of PCE degradation appeared unaffected by

Fe(III) respiration by FeRB, which may be due to Fe(III) bioavailability and the low Fe(III) respiration rate. Sulfate respiration by SRB did delay and decrease the PCE degradation rate; however, as was seen in the 3-part community simulation, this effect was moderated by the presence of FeRB.

The focus of the study was one-step dehalorespiration of PCE, however the experimental design and modeling tool could be extended to more complex systems, such as multi-step degradation of chlorinated ethenes and investigation of microbial competition during the transformation of further PCE daughter products *cis*-dichloroethene and vinyl chloride. The number of guilds considered could be expanded to include, for instance, fermenting organisms. Both the experimental and modeling approach can be adapted to investigate degradation of different organic contaminants and microbial community interactions in two-, three-, and four-phase systems and with sample removal not limited to the aqueous phase. For instance, volatile compounds may be sampled and measured directly from the gaseous phase.

The modeling tool developed in this study has a flexible structure that can be easily transferable to other domains with different properties and dimensionality. For instance the reaction modules developed in this work could be adapted to investigate community interactions between the same microbial guilds and the feedback effects of aquatic chemistry in flow-through microcosms (Bauer et al., 2009b). This will allow exploring the combined effects of solute transport processes, geochemical reactions, contaminant degradation and ecological interactions in multidimensional systems in which the physical and chemical heterogeneity will impact the biogeochemical processes and the spatial distribution of different bacterial guilds in flow-through porous media. Similarly, the reaction modules that describe microbial community and biogeochemical interactions could be applied in reactive transport simulators at the field scale to help interpret the behavior of

groundwater contaminant plumes (e.g., Parker et al., 2008; Shani et al., 2013; Van Breukelen and Rolle, 2012).

### Declaration of interests

The authors declare that they have no known competing financial interests or personal relationships that could have appeared to influence the work reported in this paper.

### Acknowledgements

This study was funded by a DTU alliance PhD scholarship granted to Alexandra Murray. Massimo Rolle acknowledges the support of the Independent Research Fund Denmark (grant DFF-7017-00130). Constructive comments from two anonymous reviewers helped to improve the quality of the manuscript.

### Appendix A. Supplementary data

Supplementary data to this article can be found online at <https://doi.org/10.1016/j.watres.2019.05.087>.

### References

- Abe, Y., Aravena, R., Zopfi, J., Parker, B., Hunkeler, D., 2009. Evaluating the fate of chlorinated ethenes in streambed sediments by combining stable isotope, geochemical and microbial methods. *J. Contam. Hydrol.* 107, 10–21. <https://doi.org/10.1016/j.jconhyd.2009.03.002>.
- Aeppli, C., Berg, M., Cirpka, O.A., Holliger, C., Schwarzenbach, R.P., Hofstetter, T.B., 2009. Influence of mass-transfer limitations on carbon isotope fractionation during microbial dechlorination of trichloroethene. *Environ. Sci. Technol.* 43, 8813–8820. <https://doi.org/10.1021/es901481b>.
- Amos, B.K., Christ, J.A., Abriola, L.M., Pennell, K.D., Löffler, F.E., 2007. Experimental evaluation and mathematical modeling of microbially enhanced tetrachloroethene (PCE) dissolution. *Environ. Sci. Technol.* 41, 963–970. <https://doi.org/10.1021/es061438n>.
- Appelo, C.A.J., Postma, D., 2005. In: A.A. (Ed.), *Geochemistry, Groundwater and Pollution*, Second. Balkema Publishers, Leiden.
- Aulenta, F., Beccari, M., Majone, M., Papini, M.P., Tandoi, V., 2008. Competition for H<sub>2</sub> between sulfate reduction and dechlorination in butyrate-fed anaerobic cultures. *Process Biochem.* 43, 161–168. <https://doi.org/10.1016/j.procbio.2007.11.006>.
- Aulenta, F., Pera, A., Rossetti, S., Petrangeli Papini, M., Majone, M., 2007. Relevance of side reactions in anaerobic reductive dechlorination microcosms amended with different electron donors. *Water Res.* 41, 27–38. <https://doi.org/10.1016/j.watres.2006.09.019>.
- Badziong, W., Thauer, R.K., 1978. Growth yields and growth rates of *Desulfovibrio vulgaris* (Marburg) growing on hydrogen plus sulfate and hydrogen plus thio-sulfate as the sole energy sources. *Arch. Microbiol.* 117, 209–214. <https://doi.org/10.1007/bf00402310>.
- Balkwill, D.L., Leach, F.R., Wilson, J.T., McNabb, J.F., White, D.C., 1988. Equivalence of Microbial Biomass Measures Based on Membrane Lipid and Cell Wall Components, Adenosine Triphosphate, and Direct Counts in Subsurface Aquifer Sediments Abstract, pp. 73–84.
- Bauer, R.D., Rolle, M., Bauer, S., Eberhardt, C., Grathwohl, P., Kolditz, O., Meckenstock, R.U., Griebler, C., 2009a. Enhanced biodegradation by hydraulic heterogeneities in petroleum hydrocarbon plumes. *J. Contam. Hydrol.* 105, 56–68. <https://doi.org/10.1016/j.jconhyd.2008.11.004>.
- Bauer, R.D., Rolle, M., Kürzinger, P., Grathwohl, P., Meckenstock, R.U., Griebler, C., 2009b. Two-dimensional flow-through microcosms – versatile test systems to study biodegradation processes in porous aquifers. *J. Hydrol.* 369, 284–295. <https://doi.org/10.1016/j.jhydrol.2009.02.037>.
- Berggren, D.R.V., Marshall, I.P.G., Azizian, M.F., Spormann, A.M., Semprini, L., 2013. Effects of sulfate reduction on the bacterial community and kinetic parameters of a dechlorinating culture under chemostat growth conditions. *Environ. Sci. Technol.* 47, 1879–1886. <https://doi.org/10.1021/es304244z>.
- Buchner, D., Jin, B., Ebert, K., Rolle, M., Elsner, M., Haderlein, S.B., 2016. Experimental determination of isotope enrichment factors – bias from mass removal by repetitive sampling. *Environ. Sci. Technol.* [acs.est.6b03689](https://doi.org/10.1021/acs.est.6b03689) <https://doi.org/10.1021/acs.est.6b03689>.
- Butt, G.F., Holliger, C., Maillard, J., 2013. Functional genotyping of *Sulfurospirillum* spp. in mixed cultures allowed the identification of a new tetrachloroethene reductive dehalogenase. *Appl. Environ. Microbiol.* 79. <https://doi.org/10.1128/AEM.02312-13>.
- Butt, G.F., Murray, A.M., Goris, T., Burion, M., Jin, B., Rolle, M., Holliger, C., Maillard, J., 2018. Coexistence of two distinct *Sulfurospirillum* populations respiring tetrachloroethene-genomic and kinetic considerations. *FEMS Microbiol. Ecol.* 94, 1–11. <https://doi.org/10.1093/femsec/fiy018>.
- Chambon, J.C., Bjerg, P.L., Scheutz, C., Bælum, J., Jakobsen, R., Binning, P.J., 2013. Review of reactive kinetic models describing reductive dechlorination of chlorinated ethenes in soil and groundwater. *Biotechnol. Bioeng.* 110, 1–23. <https://doi.org/10.1002/bit.24714>.
- Charlton, S.R., Parkhurst, D.L., 2011. Modules based on the geochemical model PHREEQC for use in scripting and programming languages. *Comput. Geosci.* 37, 1653–1663. <https://doi.org/10.1016/j.cageo.2011.02.005>.
- Cypionka, H., 2000. Oxygen respiration by *Desulfovibrio* species. *Annu. Rev. Microbiol.* 54, 827–848.
- Daugulis, A.J., 2001. Two-phase partitioning bioreactors: a new technology platform for destroying xenobiotics. *Trends Biotechnol.* 19, 457–462. [https://doi.org/10.1016/S0167-7799\(01\)01789-9](https://doi.org/10.1016/S0167-7799(01)01789-9).
- Déziel, E., Comeau, Y., Villemur, R., 1999. Two-liquid-phase bioreactors for enhanced degradation of hydrophobic/toxic compounds. *Biodegradation* 10, 219–233. <https://doi.org/10.1023/A:1008311430525>.
- Elias, D.A., Sullita, J.M., McInerney, M.J., Krumholz, L.R., 2004. Periplasmic Cytochrome c3 of *Desulfovibrio vulgaris* is directly involved in H<sub>2</sub>-mediated metal but not sulfate reduction. *Appl. Environ. Microbiol.* 70, 413–420. <https://doi.org/10.1128/AEM.70.1.413>.
- Fredrickson, J.K., Romine, M.F., Beliaev, A.S., Auchtung, J.M., Driscoll, M.E., Gardner, T.S., Nealon, K.H., Osterman, A.L., Pinchuk, G., Reed, J.L., Rodionov, D., Rodrigues, J.L.M., Saffarini, D., Serres, M.H., Spormann, A.M., Zhulin, I.B., Tiedje, J.M., 2008. Towards environmental systems biology of *Shewanella*. *Nat. Rev. Microbiol.* 6, 592–603. <https://doi.org/10.1038/nrmicro1947>.
- Gadd, G.M., 2010. Metals, minerals and microbes: geomicrobiology and bioremediation. *Microbiol.* 156, 609–643. <https://doi.org/10.1099/mic.0.037143-0>.
- Haas, J.R., Dichristina, T.J., 2002. Effects of Fe(III) chemical speciation on dissimilatory Fe(III) reduction by *Shewanella putrefaciens*. *Environ. Sci. Technol.* 36, 373–380. <https://doi.org/10.1021/es0109287>.
- Haberer, C.M., Muniruzzaman, M., Grathwohl, P., Rolle, M., 2015. Diffusive-dispersive and reactive fronts in porous media: iron(II) oxidation at the unsaturated-saturated interface. *Vadose Zone J.* 14, 1–14. <https://doi.org/10.2136/vzj2014.07.0091>.
- Hamonts, K., Kuhn, T., Vos, J., Maesen, M., Kalka, H., Smidt, H., Springael, D., Meckenstock, R.U., Dejonghe, W., 2012. Temporal variations in natural attenuation of chlorinated aliphatic hydrocarbons in eutrophic river sediments impacted by a contaminated groundwater plume. *Water Res.* 46, 1873–1888. <https://doi.org/10.1016/j.watres.2012.01.001>.
- Heidelberg, J.F., Paulsen, I.T., Nelson, K.E., Gaidos, E.J., Nelson, W.C., Read, T.D., Eisen, J. A., Seshadri, R., Ward, N., Methe, B., Clayton, R. a, Meyer, T., Tsapin, A., Scott, J., Beanan, M., Brinkac, L., Daugherty, S., DeBoy, R.T., Dodson, R.J., Durkin, A. S., Haft, D.H., Kolonay, J.F., Madupu, R., Peterson, J.D., Umayam, L. a, White, O., Wolf, A.M., Vamathevan, J., Weidman, J., Impraim, M., Lee, K., Berry, K., Lee, C., Mueller, J., Khouri, H., Gill, J., Utterback, T.R., McDonald, L. a, Feldblyum, T.V., Smith, H.O., Venter, J.C., Nealon, K.H., Fraser, C.M., 2002. Genome sequence of the dissimilatory metal ion-reducing bacterium *Shewanella oneidensis*. *Nat. Biotechnol.* 20, 1118–1123. <https://doi.org/10.1038/nbt749>.
- Heidelberg, J.F., Seshadri, R., Haveman, S.A., Hemme, C.L., Paulsen, I.T., Kolonay, J.F., Eisen, J.A., Ward, N., Methe, B., Brinkac, L.M., Daugherty, S.C., Deboy, R.T., Dodson, R.J., Durkin, A.S., Madupu, R., Nelson, W.C., Sullivan, S.A., Fouts, D., Haft, D.H., Selengut, J., Peterson, J.D., Davidsen, T.M., Zafar, N., Zhou, L., Radune, D., Dimitrov, G., Hance, M., Tran, K., Khouri, M., Gill, J., Utterback, T.R., Feldblyum, T.V., Wall, J.D., Voordouw, G., Fraser, C.M., 2004. The genome sequence of the anaerobic, sulfate-reducing bacterium *Desulfovibrio vulgaris* Hildenborough. *Nat. Biotechnol.* 22, 554–559. <https://doi.org/10.1038/nbt959>.
- Holliger, C., Schraa, G., Stams, A.J.M., Zehnder, A.J.B., 1993. A highly purified enrichment culture couples the reductive dechlorination of tetrachloroethene to growth. *Appl. Environ. Microbiol.* 59, 2991–2997.
- Imfeld, G., Nijenhuis, I., Nikolausz, M., Zeiger, S., Paschke, H., Drangmeister, J., Grossmann, J., Richnow, H.H., Weber, S., 2008. Assessment of in situ degradation of chlorinated ethenes and bacterial community structure in a complex contaminated groundwater system. *Water Res.* 42, 871–882. <https://doi.org/10.1016/j.watres.2007.08.035>.
- Jakobsen, R., 2007. Redox microniches in groundwater: a model study on the geometric and kinetic conditions required for concomitant Fe oxide reduction, sulfate reduction, and methanogenesis. *Water Resour. Res.* 43. <https://doi.org/10.1029/2006WR005663>.
- Jin, B., Haderlein, S.B., Rolle, M., 2013. Integrated carbon and chlorine isotope modeling: applications to chlorinated aliphatic hydrocarbons dechlorination. *Environ. Sci. Technol.* 47, 1443–1451. <https://doi.org/10.1021/es304053h>.
- Jin, B., Rolle, M., 2016. Joint interpretation of enantiomer and stable isotope fractionation for chiral pesticides degradation. *Water Res.* 105, 178–186. <https://doi.org/10.1016/j.watres.2016.08.057>.
- Kampana, M., Thullner, M., Richnow, H.H., Harms, H., Wick, L.Y., 2008. Impact of bioavailability restrictions on microbially induced stable isotope fractionation. 2. Experimental evidence. *Environ. Sci. Technol.* 42, 6544–6551. <https://doi.org/10.1021/Es702781x>.
- Kotik, M., Davidová, A., Vorišková, J., Baldrian, P., 2013. Bacterial communities in tetrachloroethene-polluted groundwaters: a case study. *Sci. Total Environ.* 454, 517–527. <https://doi.org/10.1016/j.scitotenv.2013.02.082>.
- Kouznetsova, I., Mao, X., Robinson, C., Barry, D. a., Gerhard, J.L., McCarty, P.L., 2010. Biological reduction of chlorinated solvents: batch-scale geochemical modeling. *Adv. Water Resour.* 33, 969–986. <https://doi.org/10.1016/j.advwatres.2010.04.017>.

- Liu, C., Zachara, J.M., Gorby, Y.A., Szecsody, J.E., Brown, C.F., 2001. Microbial reduction of Fe(III) and sorption/precipitation of Fe(II) on *Shewanella putrefaciens* strain CN32. *Environ. Sci. Technol.* 35, 1385–1393. <https://doi.org/10.1021/es0015139>.
- Malaguerra, F., Chambon, J.C., Bjerg, P.L., Scheutz, C., Binning, P.J., 2011. Development and sensitivity analysis of a fully kinetic model of sequential reductive dechlorination in groundwater. *Environ. Sci. Technol.* 45, 8395–8402. <https://doi.org/10.1021/es201270z>.
- Mao, X., Stenuit, B., Polasko, A., Alvarez-Cohen, L., 2015. Efficient metabolic exchange and electron transfer within a syntrophic trichloroethene-degrading coculture of *Dehalococcoides mccartyi* 195 and *Syntrophomonas wolfei*. *Appl. Environ. Microbiol.* 81, 2015–2024. <https://doi.org/10.1128/AEM.03464-14>.
- Marcus, I.M., Wilder, H.A., Quazi, S.J., Walker, S.L., 2013. Linking microbial community structure to function in representative simulated systems. *Appl. Environ. Microbiol.* 79, 2552–2559. <https://doi.org/10.1128/AEM.03461-12>.
- Meckenstock, R.U., Elsner, M., Griebler, C., Lueders, T., Stumpp, C., Dejonghe, W., Bastiaens, L.L., Springael, D., Smolders, E., Boon, N., Agathos, S.N., Sorensen, S.R., Amand, J., Albrechtsen, H.J., Bjerg, P.L., Schmidt, S., Huang, W.E., Van Breukelen, B.M., 2015. Biodegradation: updating the concepts of control for microbial clean-up in contaminated aquifers. *Environ. Sci. Technol.* 49, 7073–7081. <https://doi.org/10.1021/acs.est.5b00715>.
- Muniruzzaman, M., Rolle, M., 2016. Modeling multicomponent ionic transport in groundwater with IPHreeqc coupling: electrostatic interactions and geochemical reactions in homogeneous and heterogeneous domains. *Adv. Water Resour.* 98, 1–15. <https://doi.org/10.1016/j.advwatres.2016.10.013>.
- Noguera, D., Brusseau, G., Rittmann, B., Stahl, D., 1998. A unified model describing the role of hydrogen in the growth of *Desulfovibrio vulgaris* under different environmental conditions. *Biotechnol. Bioeng.* 59, 732–746. [https://doi.org/10.1002/\(sici\)1097-0290\(19980920\)59:6<732::aid-bit10>3.3.co;2-2](https://doi.org/10.1002/(sici)1097-0290(19980920)59:6<732::aid-bit10>3.3.co;2-2).
- Park, H.S., Lin, S., Voordouw, G., 2008. Ferric iron reduction by *Desulfovibrio vulgaris* Hildenborough wild type and energy metabolism mutants. *Antonie van Leeuwenhoek. Int. J. Gen. Mol. Microbiol.* 93, 79–85. <https://doi.org/10.1007/s10482-007-9181-3>.
- Parker, B.L., Chapman, S.W., Guilbeault, M.A., 2008. Plume persistence caused by back diffusion from thin clay layers in a sand aquifer following TCE source-zone hydraulic isolation. *J. Contam. Hydrol.* 102, 86–104. <https://doi.org/10.1016/j.jconhyd.2008.07.003>.
- Parkhurst, D.L., Appelo, C.A.J., 2013. Description of input and examples for PHREEQC Version 3 — a computer program for speciation, batch-reaction, one-dimensional transport, and inverse geochemical calculations. U.S. Geol. Surv. Tech. Methods, B. 6 chapter A43 6–43A. [https://doi.org/10.1016/0029-6554\(94\)90020-5](https://doi.org/10.1016/0029-6554(94)90020-5).
- Postma, D., Jakobsen, R., 1996. Redox zonation: equilibrium constraints on the Fe(III)/SO<sub>4</sub>-reduction interface. *Geochem. Cosmochim. Acta* 60, 3169–3175.
- Poulton, S.W., Krom, M.D., Raiswell, R., 2004. A revised scheme for the reactivity of iron (oxyhydr) oxide minerals towards dissolved sulfide. *Geochem. Cosmochim. Acta* 68, 3703–3715. <https://doi.org/10.1016/j.gca.2004.03.012>.
- Prommer, H., Anneser, B., Rolle, M., Einsiedl, F., Griebler, C., 2009. Biogeochemical and isotopic gradients in a BTEX/PAH contaminant plume: model-based interpretation of a high-resolution field data set. *Environ. Sci. Technol.* 43, 8206–8212. <https://doi.org/10.1021/es901142a>.
- Remoundaki, E., Kousi, P., Joulain, C., Battaglia-Brunet, F., Hatzikioseyian, A., Tsezos, M., 2008. Characterization, morphology and composition of biofilm and precipitates from a sulphate-reducing fixed-bed reactor. *J. Hazard Mater.* 153, 514–524. <https://doi.org/10.1016/j.jhazmat.2007.08.094>.
- Rickard, D., 1995. Kinetics of FeS precipitation: Part 1. Competing reaction mechanisms. *Geochem. Cosmochim. Acta* 59, 4367–4379. [https://doi.org/10.1016/0016-7037\(95\)00251-T](https://doi.org/10.1016/0016-7037(95)00251-T).
- Rickard, D., Luther, G.W., 2007. Chemistry of iron sulfides, chemical reviews. <https://doi.org/10.1021/cr0503658>.
- Rittmann, B.E., McCarty, P.L., 2001. *Environmental Biotechnology: Principles and Applications*, First. ed. McGraw-Hill, New York.
- Rolle, M., Chiogna, G., Bauer, R., Griebler, C., Grathwohl, P., 2010. Isotopic fractionation by transverse dispersion: flow-through microcosms and reactive transport modeling study. *Environ. Sci. Technol.* 44, 6167–6173. <https://doi.org/10.1021/es101179f>.
- Rolle, M., Kitanidis, P.K., 2014. Effects of compound-specific dilution on transient transport and solute breakthrough: a pore-scale analysis. *Adv. Water Resour.* 71, 186–199. <https://doi.org/10.1016/j.advwatres.2014.06.012>.
- Rolle, M., Sprocati, R., Masi, M., Jin, B., Muniruzzaman, M., 2018. Nernst-Planck-based description of transport, coulombic interactions, and geochemical reactions in porous media: modeling approach and benchmark experiments. *Water Resour. Res.* 54, 3176–3195. <https://doi.org/10.1002/2017WR022344>.
- Schneidewind, U., Haest, P.J., Atashgahi, S., Maphosa, F., Hamonts, K., Maesen, M., Calderer, M., Seuntjens, P., Smidt, H., Springael, D., Dejonghe, W., 2014. Kinetics of dechlorination by *Dehalococcoides mccartyi* using different carbon sources. *J. Contam. Hydrol.* 157, 25–36. <https://doi.org/10.1016/j.jconhyd.2013.10.006>.
- Scholz-Muramatsu, H., Neumann, A., Messmer, M., Moore, E., Diekert, G., 1995. Isolation and characterization of *Dehalospirillum multivorans* gen. nov., sp. nov., a tetrachloroethene-utilizing, strictly anaerobic bacterium. *Arch. Microbiol.* 163, 48–56.
- Shani, N., Rossi, P., Holliger, C., 2013. Correlations between environmental variables and bacterial community structures suggest Fe(III) and vinyl chloride reduction as antagonistic terminal electron-accepting processes. *Environ. Sci. Technol.* 47, 6836–6845. <https://doi.org/10.1021/es304017s>.
- Tang, Y.J., Meadows, A.L., Keasling, J.D., 2007. A kinetic model describing *Shewanella oneidensis* MR-1 growth, substrate consumption, and product secretion. *Biotechnol. Bioeng.* 96, 125–133. <https://doi.org/10.1002/bit>.
- Tao, X., Li, Y., Huang, H., Chen, Y., Liu, P., Li, X., 2014. *Desulfovibrio vulgaris* Hildenborough prefers lactate over hydrogen as electron donor. *Ann. Microbiol.* 64, 451–457. <https://doi.org/10.1007/s13213-013-0675-0>.
- Thullner, M., Fischer, A., Richnow, H.H., Wick, L.Y., 2012. Influence of mass transfer on stable isotope fractionation. *Appl. Microbiol. Biotechnol.* 97, 441–452. <https://doi.org/10.1007/s00253-012-4537-7>.
- Thullner, M., Kampara, M., Richnow, H.H., Harms, H., Wick, L.Y., 2008. Impact of bioavailability restrictions on microbially induced stable isotope fractionation. 1. Theoretical calculation. *Environ. Sci. Technol.* 42, 6544–6551. <https://doi.org/10.1021/Es702781x>.
- Van Breukelen, B.M., Rolle, M., 2012. Transverse hydrodynamic dispersion effects on isotope signals in groundwater chlorinated solvents plumes. *Environ. Sci. Technol.* 46, 7700–7708. <https://doi.org/10.1021/es301058z>.
- Van Breukelen, B.M., Thouement, H.A.A., Stack, P.E., Vanderford, M., Philp, P., Kuder, T., 2017. Modeling 3D-CSIA data: carbon, chlorine, and hydrogen isotope fractionation during reductive dechlorination of TCE to ethene. *J. Contam. Hydrol.* 204, 79–89. <https://doi.org/10.1016/j.jconhyd.2017.07.003>.
- Viollier, E., Inglett, P.W., Hunter, K., Roychoudhury, A.N., Van Cappellen, P., 2000. The ferrozinc method revisited: Fe(II)/Fe(III) determination in natural waters. *Appl. Geochem.* 15, 785–790. [https://doi.org/10.1016/S0883-2927\(99\)00097-9](https://doi.org/10.1016/S0883-2927(99)00097-9).
- Wade, M.J., Harmand, J., Benyahia, B., Bouchez, T., Chaillou, S., Cloez, B., Godon, J.J., Moussa Boudjema, B., Rapaport, A., Sari, T., Arditi, R., Lobry, C., 2016. Perspectives in mathematical modelling for microbial ecology. *Ecol. Model.* 321, 64–74. <https://doi.org/10.1016/j.ecolmodel.2015.11.002>.
- Weatherill, J.J., Atashgahi, S., Schneidewind, U., Krause, S., Ullah, S., Cassidy, N., Rivett, M.O., 2018. Natural attenuation of chlorinated ethenes in hyporheic zones: a review of key biogeochemical processes and in-situ transformation potential. *Water Res.* 128, 362–382. <https://doi.org/10.1016/j.watres.2017.10.059>.
- Wells, G.F., Park, H.D., Eggleston, B., Francis, C.A., Criddle, C.S., 2011. Fine-scale bacterial community dynamics and the taxa-time relationship within a full-scale activated sludge bioreactor. *Water Res.* 45, 5476–5488. <https://doi.org/10.1016/j.watres.2011.08.006>.
- Wissmeier, L., Barry, D.A., 2011. Simulation tool for variably saturated flow with comprehensive geochemical reactions in two- and three-dimensional domains. *Environ. Model. Softw.* 26, 210–218. <https://doi.org/10.1016/j.envsoft.2010.07.005>.
- Xu, G., Lu, Q., Yu, L., Wang, S., 2019. Tetrachloroethene primes reductive dechlorination of polychlorinated biphenyls in a river sediment microcosm. *Water Res.* 152, 87–95. <https://doi.org/10.1016/j.watres.2018.12.061>.
- Yu, S., Semprini, L., 2004. Kinetics and modeling of reductive dechlorination at high PCE and TCE concentrations. *Biotechnol. Bioeng.* 88, 451–464. <https://doi.org/10.1002/bit.20260>.
- Yu, S., Semprini, L., 2002. Comparison of trichloroethylene reductive dehalogenation by microbial communities stimulated on silicon-based organic compounds as slow-release anaerobic substrates. *Water Res.* 36, 4985–4996. [https://doi.org/10.1016/S0043-1354\(02\)00222-1](https://doi.org/10.1016/S0043-1354(02)00222-1).
- Zhou, C., Vannela, R., Hayes, K.F., Rittmann, B.E., 2014. Effect of growth conditions on microbial activity and iron-sulfide production by *Desulfovibrio vulgaris*. *J. Hazard Mater.* 272, 28–35. <https://doi.org/10.1016/j.jhazmat.2014.02.046>.
- Zhou, C., Zhou, Y., Rittmann, B.E., 2017. Reductive precipitation of sulfate and soluble Fe(III) by *Desulfovibrio vulgaris*: electron donor regulates intracellular electron flow and nano-FeS crystallization. *Water Res.* 119, 91–101. <https://doi.org/10.1016/j.watres.2017.04.044>.